FLOW AND SELF-EXCITED OSCILLATIONS IN COLLAPSIBLE TUBES

Timothy J. Pedley
Department of Applied Mathematics and Theoretical Physics,
University of Cambridge
Wilberforce Road, Cambridge CB3 0WA, UK
t.j.pedley@damtp.cam.ac.uk

ABSTRACT

Laboratory experiments designed to shed light on fluid flow through collapsible tubes, a problem with several physiological applications, invariably give rise to a wide variety of self-excited oscillations. This talk surveys the background and then outlines a two-dimensional model that has been developed to describe the standard experiment, of flow along a finite length of elastic tube mounted at its ends on rigid tubes and contained in a chamber whose pressure can be independently varied. The configuration is that of flow in a parallel-sided channel with a segment of one wall replaced by a membrane under longitudinal tension T. In the absence of bending stiffness the flow and membrane displacement have been calculated using an unsteady Navier-Stokes computation.

For a given Reynolds number, Re, steady flow becomes unstable when T falls below a critical value (equivalently, when Re exceeds a critical value for fixed T), and the consequent oscillations reveal at least one period-doubling bifurcation as T is further reduced. The effect of wall inertia has also been investigated: it is negligible if the flowing fluid is water, but leads to an independent, high frequency flutter when it is air. The most recent version of the computations incorporates elongational and bending stiffness, and a surprising finding is that a narrow band of stable states occurs in the middle of an otherwise unstable region of parameter space.

1. INTRODUCTION

1.1 Collapse

Any elastic tube will collapse if it is squeezed hard enough. If a long segment of uniform elastic tube is subjected to different levels of transmural (internal minus external) pressure, p_{tm}, the cross-sectional shape and area, A, will vary as sketched in Figure 1. When p_{tm} is large and positive, the cross-section will be circular and rather stiff because the perimeter must be stretched in order to increase A. As p_{tm} is lowered, a critical value is passed at which the circular cross-section buckles, becoming at first elliptical and then more significantly deformed. During this phase a thin-walled tube is very compliant (large area change for small pressure change) because only wall bending is required for a change of shape and hence area. At very low values of A the tube is almost totally collapsed and becomes stiff again. During the compliant phase, even the small pressure changes associated with flow through the tube (viscous or inertial) can be enough to cause collapse.

The collapse of compressed elastic tubes conveying a flow occurs naturally in several physiological applications. Examples include: (i) Blood flow in veins, either above the level of the heart where the internal pressure may be subatmospheric because of the effect of gravity (the jugular vein of the giraffe is particularly interesting in this context: Pedley, Brook & Seymour (1996); Brook, Falle & Pedley (1999)), or being squeezed by contracting skeletal muscle as in the "muscle pump" used to return blood to the heart from the feet of an upright mammal. (ii) Blood flow in arteries, such as intra-myocardial coronary arteries during the contraction of the left ventricle, or actively squeezed by an external agency such as a blood pressure cuff. (iii) Air flow in the large intrathoracic airways of the lung during a forced expiration or cough, because an increase in alveolar air pressure, intended to increase the expiratory flow rate, is also exerted on the outside of the airways. In this case, increasing alveolar pressure above a certain level does not increase the expiratory flow rate, a process known as *flow limitation*. (4) Urine flow in the urethra during micturition, where flow limitation is again commonplace. These and other examples are discussed in greater detail by Shapiro (1977 a,b). Note that in all the cases mentioned the Reynolds number of the flow (Re) is in the hundreds or higher.

1.2 In vitro experiments

Many workers have performed laboratory experiments on nominally steady flow through collapsible tubes. In the standard experiment a segment of collapsible (e.g. rubber) tube is mounted at its ends on rigid tubes and contained in a chamber whose pressure, p_e, can be independently controlled; the behaviour of the system depends on two independent pressure *differences*, e.g. $p_u - p_d$ and $p_e - p_d$, where p_u and p_d are pressure far upstream and downstream. Some early experimental studies sought to characterise the collapsible tube by plotting the pressure difference along it ($\Delta p = p_1 - p_2$: see Figure 2) against the flow-rate, q; there was some confusion in the literature because it was not always clear which controlled pressure difference was being varied, as flow rate was varied, and which was held constant. Three different examples, in each of which the shape of the $\Delta p - q$ curve is quite different, are shown in Figure 3 (a,b,c), taken from Brecher (1952), Bertram (1986) and Conrad (1969), respectively. The following explanations of the three different curves are taken from Kamm & Pedley (1989).

For the case depicted in figure 3(a), $p_1 - p_2$ is increased while $p_1 - p_e$ is held constant. This can be accomplished either by reducing p_2 with p_1 and p_e fixed, or by simultaneously increasing p_1 and p_e while p_2 is held constant. With either manoeuvre, q at first increases but above a critical value it levels off and exhibits flow limitation: however much the driving pressure is increased the flow rate remains constant or may

even fall as a result of increasingly severe tube collapse. This version of the experiment is directly relevant to forced expiration from the lung (Elad & Kamm, 1989; Lambert, 1989) to venous return (Guyton, 1962) and to micturition (Griffiths, 1971).

Different results are obtained if $p_1 - p_2$ or q is increased while $p_2 - p_e$ is held constant at some negative value (Fry, 1958; Brower & Noordergraaf, 1973; Bonis & Ribreau, 1978). In this case the tube is collapsed at low flow rates, but starts to open up from the upstream end as q increases above a critical value, so that the resistance falls and $p_1 - p_2$ ceases to rise; so called "pressure-drop limitation" (figure 3(b)). This experiment is not directly applicable to any particular physiological condition, but it turns out that $p_2 - p_e$ is a natural control parameter for at least one of the types of theoretical model that have been proposed (Shapiro, 1977a). Figure 3(b) represents some experimental results of pressure flow relations for several values of $p_e - p_2$ (Bertram et al, 1990).

In a third type of experiment, $p_1 - p_2$ is held constant while $p_2 - p_e$ is decreased from a large positive value. The tube first behaves as though it were rigid and the flow rate is nearly constant. Then as $p_2 - p_e$ becomes sufficiently negative to produce partial collapse, the resistance rises and q begins to fall. This is analogous to what happens in the pulmonary capillaries near the apex of the lung (Permutt et al, 1963). One notable variation on these experiments is that pioneered by Conrad (1969) who held p_e constant and the pressure downstream of the collapsible segment but upstream of a flow resistance, p_2, varies with q as does the degree of tube collapse. Thus at high flow rates the tube is distended and its resistance is low, but as the flow rate is reduced below a critical value the tube starts to collapse and its resistance and $p_1 - p_2$ increase as q is decreased. Only when the tube is severely collapsed along most of its length does $p_1 - p_2$ start to decrease again as q approaches zero (figure 3(c)).

In almost all such collapsible tube experiments with $Re >$ about 200, ranges of parameters were found in which steady flow could not be achieved but, instead, large-amplitude, flow-induced oscillations were observed. Bertram and his colleagues (1982,1986,1990,1991) have made probably the most systematic series of experiments on self-excited oscillations in collapsible tubes, recording as functions of time the pressures (p_1, p_2) and flow rates (q_1, q_2) at the upstream and downstream ends of the collapsible segment, and the cross-sectional area A_n at the narrowest point. Examples of some of the measurements of $p_2(t)$ for various parameter values are shown in Figure 4; a great variety of oscillatory behaviour is exhibited. Bertram, et al. (1990) have tried to map out the associated control space diagrams, to identify regions in which different types of oscillation arise. All that can be said in summary is that a finite length of compressed collapsible tube conveying a flow represents a dynamical system of remarkable richness and complexity. It would clearly be of great interest to be able to model the system theoretically and hence understand it physically. That interest is independent of any physiological relevance, though it should be noted that flow-induced oscillations do arise in some of the physiological applications: wheezing during forced expiration; the Korotkov sounds listened for during blood pressure measurement with a cuff; and "cervical venous hum" (Danaky & Ronan, 1974) are but three examples.

2. ONE-DIMENSIONAL MODELS

2.1 Basic equations

The earliest and simplest theoretical models of collapsible-tube flow were lumped-parameter or zero-dimensional models, in which the relevant variables were functions only of time t, and satisfied nonlinear ordinary differential equations. The geometry of the whole collapsible segment would be represented, say, by the cross-sectional area at the narrowest point, $A_n(t)$, and the other variables would be the pressure at that point, $p_n(t)$, together with the measurable quantities $p_1(t), p_2(t), q_1(t), q_2(t)$. The variables were linked by dynamical equations representing conservation of mass and momentum, together with a *tube law* (Figure 1) relating the transmural pressure $p_n - p_e$ and the area A_n, but only at the narrowest point. The system of ordinary differential equations was typically of second or third order (Conrad (1969), Schoendorfer & Shapiro (1977), Pedley (1980, Chapter 6), Bertram & Pedley (1983)), though the well-known model of Katz, Chen & Moreno (1969) was of fifth order. Some authors, in the days before modern dynamical systems theory, were content to imply that, since both their experiments and their model produced oscillations, the problem was solved. Because many real mechanical features cannot be incorporated in lumped-parameter models, we do not discuss them further here.

The next level of sophistication is a one-dimensional model, in which the pressure p and the longitudinal velocity u, both averaged across the tube cross-section, together with the cross-sectional area A, are regarded as functions of the longitudinal coordinate x and time t. The governing equations have traditionally been taken to be the following (Shapiro, 1977a):

$$\text{conservation of mass} \quad \frac{\partial A}{\partial t} + \frac{\partial (uA)}{\partial x} = 0 \tag{1}$$

$$\text{conservation of momentum} \quad \frac{\partial u}{\partial t} + u\frac{du}{dx} = -\frac{1}{\rho}\frac{dp}{dx} - \frac{R(A,u)uA}{\rho} \tag{2}$$

$$\text{elasticity (tube law)} \quad p - p_e = \tilde{P}(A) \tag{3}$$

where the function $\tilde{P}(A)$ represents the tube law (figure 1). In equation (2) the body force term has been omitted since the longitudinal component of gravity is equivalent to a gradient in external pressure,p_e. The convective inertia term does not include the contribution from the non-flat velocity profile, which can in general be incorporated into the term, RuA, representing viscous resistance; R is assumed to be positive, and increases rapidly as A decreases. The set of equations (1)-(3) are exactly analogous to those for water flow in shallow channels with a free surface.

An interesting application of the above one-dimensional equations is provided by blood flow in the giraffe jugular vein: see Pedley et al (1996), Brook et al (1999), Brook & Pedley (2002). I shall not repeat those studies here, except in the following brief summary:

> The giraffe has a neck of phenomenal length
> Up which blood must be pumped to the brain.
> The consequence is a heart of great strength
> And collapse of the jugular vein.

2.2 Modelling the laboratory experiments

Instead we consider the experiment depicted in figure 2, with the tube horizontal, and see how well it can be described by the one-dimensional theory. We again consider steady flow, so the governing equations are (3), plus the time-independent versions of (1) and (2). Eliminating p we obtain:

$$\frac{1}{A}\frac{dA}{dx} = \frac{R(A)q}{\rho(c^2 - u^2)}, \tag{4}$$

where

$$c^2 = \frac{A}{\rho}\frac{d\tilde{P}}{dA}$$

Note that $c(A)$ is the speed at which small amplitude pressure waves propagate along the tube, in the absence of through flow, when its cross-sectional area is uniformly equal to A (Shapiro, 1977a) and q is the flow-rate uA (constant). Suppose that, at an upstream station, the tube is circular and $u < c$. dA/dx is negative, so A decreases (tending to reduce c) while u increases because uA is constant. Thus dA/dx becomes increasingly negative and, if the tube is long enough, a choke point will be reached at which u is predicted to be equal to c and $dA/dx = -\infty$. By this stage the steady flow model will clearly have broken down: steady flow at the proposed flow rate q, from the postulated upstream conditions, is not possible. If q and the upstream area are held fixed, and the model is a correct one for steady flow, then unsteady behaviour must follow. A number of authors (e.g. Brower & Scholten, 1975) have gone further and suggested that the presence of a point at which the fluid speed is equal to the wave speed is the prime mechanism for the initiation of unsteady behaviour - i.e. of self-excited oscillations.

However, the one-dimensional model contained in equations (1)-(3) must break down anyway, even without choking, in order to describe the experiment depicted in figure 2, because dA/dx would have to become positive again near the downstream end $x = \ell$. Cancelli & Pedley (1985) added two new features, both of which should be important in the region downstream of the narrowest point. One was longitudinal tension in the tube wall, the simplest model for which causes equation (3) to be replaced by

$$p - p_e = \tilde{P}(A) - T\frac{D^2 A}{dx^2}. \tag{5}$$

In the highly collapsed region the tube wall resembles two flattish membranes under tension, with longitudinal curvature roughly proportional to d^2A/dx^2. It was felt that the addition of extra x-derivatives would enable more boundary conditions to be applied, such as $A(\ell) = A(0) = A_0$. The other new feature was the recognition that flow through a constriction will separate, a process leading to enhanced energy loss and therefore substantially incomplete pressure recovery in the region downstream of the narrowest point. The energy loss downstream of the narrowest point had already been identified as important in lumped-parameter models (Pedley, 1980). Cancelli & Pedley (1985) used momentum arguments to suggest that a reasonable, yet still simple, model of the energy loss in steady flow could be achieved by replacing the steady version of equation (2), downstream of the narrowest point, by

$$\chi u\frac{du}{dx} = 1\frac{1}{\rho}\frac{dp}{dx}, \tag{6}$$

where χ is a non-negative quantity, less than 1; in their (unsteady) calculations Cancelli & Pedley took $\chi = 0.2$.

The steady flow model described by equations (15) and (16) with $q = uA$ and

$$\tilde{P}(A) = K_p(1 - \alpha^{-3/2}) \quad \text{for} \quad \alpha < 1 \tag{7}$$

$$= K_p k(\alpha - 1) \quad \text{for} \quad \alpha > 1$$

(where $\alpha = A/A_0$) was exhaustively analysed by Jensen & Pedley (1989). These authors neglected the direct viscous term Ru, taking $\chi = 1$ for $0 < x < x_s$ (the unknown point of flow separation, taken to be identical with the narrowest point at sufficiently high Reynolds number) and $\chi =$ constant ≤ 1 for $x_s < x < \ell$. Their principal results can be summarised as follows:

(i) when $\chi = 1$ everywhere, i.e. there is no energy loss in the collapsible tube downstream of the narrowest point, then there exists a critical value of the flow rate q, dependent on the longitudinal tension T, above which the steady problem has no solution. In other words, the presence of longitudinal tension alone does not abolish choking; this should not have been a surprise: in the same way, surface tension does not abolish critical behaviour in shallow-water channel flow.

(ii) However, whenever there is any downstream-energy loss, i.e. $\chi < 1$ for $x_s < x < \ell$, then a steady solution exists for all positive values of flow rate q and tension T. Since some such energy loss is inevitable, it follows that the breakdown of steady flow is not caused by choking, i.e. the non-existence of a steady flow at the chosen parameter values, but must arise through instability of the steady solution.

Jensen (1990) gave a detailed linear, and weakly nonlinear, analysis of the instability of the steady flow. He used the same one-dimensional model with the time derivatives, $\partial A/\partial t$ and $\partial u/\partial t$, restored. The elasticity equations (5) and (7) remained unchanged. When appropriately non-dimensionalised, Jensen's model has two principal governing dimensionless parameters, in addition to χ (which was fixed at a value of 0.2 in all numerical computations): Q, which is proportional to the flow rate q, and P, proportional to the transmural pressure, $p_e - p_2$, at the downstream end of the collapsible segment when the flow is steady. Other parameters describe the resistance and inertance of the upstream and downstream rigid segments; these were kept fixed throughout. Figure 5 shows the computed stability boundaries in the $P - Q$ plane, for the first two instability modes found. The general shape, showing stable steady flow for sufficiently small P at all Q (the tube remaining effectively open), and for sufficiently small Q at all P (the tube being collapsed when P is large enough), is in qualitative agreement with the control diagrams plotted by Bertram, et al. (1990). So too are the presence of mode crossing points (i) and (ii) and the existence of several regions in parameter space in which different behaviour of the system is to be expected. Jensen's weakly nonlinear analysis showed that both modes become unstable through supercritical Hopf bifurcations everywhere except for the small segments of the stability boundaries marked as dotted in figure 5, where they are subcritical Hopf bifurcations.

In a subsequent paper Jensen (1992) showed some results of a numerical integration of the fully nonlinear one-dimensional equations, at a few selected points in parameter space, near the upper left mode crossing point in figure 5. Some of the computed time series, of $p_2(t) = p(\ell, t)$ for example, look quite

similar to the measurements of Bertram, et al (1990). It is clear that this one-dimensional model contains much that is relevant to the self-excited oscillations of real collapsible tubes in the laboratory. It would be possible to extend Jensen's (1991) full nonlinear computations to cover the whole of parameter space, and map out the behaviour in as much (or more) detail as has been done experimentally.

However, this has not been done, and should not, because of the severe *a priori* weaknesses of the one-dimensional model as a scientific description of the real system. First, the solid mechanics of equations (5) and (7) is an extremely crude representation of the nonaxisymmetric, large deformation of a cylindrical shell under pre-stretch, external pressure, and the stresses exerted by internal flow. Second, the fluid mechanics is also extremely crude, primarily because of the ad hoc way of representing flow separation and the processes of energy loss/pressure recovery downstream of the constriction. This is especially weak in unsteady flow, since the arguments leading to equation (6) were based on steady flow (Cancelli & Pedley, 1985) and take no account, for example, of the time delay between the emergence of a sufficiently adverse pressure gradient and the breakaway of previously attached flow (see the experiments of Bertram & Pedley, 1983). What is required is a solution of the unsteady, three-dimensional Navier-Stokes equations, coupled to the equations for the unsteady, three-dimensional, large-deformation theory of highly compliant shells. Numerical codes for the solution of such problems are not yet available in any branch of computational mechanics, and would require resources in excess of any available to us. Heil and his colleagues have been aproaching this goal through a series of increasingly demanding computations (Heil & Pedley (1996), Heil (1997), Hazel & Heil (2003)) but they are still some way short of a fully versatile description of self-excited oscillations.

3. TWO-DIMENSIONAL MODELS

3.1 The membrane model

Instead of attempting the full three-dimensional problem, we have sought a sound scientific solution for a simpler, two-dimensional configuration which is nevertheless in principle realisable experimentally. The configuration is sketched in figure 6. A two-dimensional channel consists of two parallel, rigid planes, distance h_0 apart, from one of which a segment of length Lh_0 has been removed and replaced by a thin membrane, with no bending stiffness or inertia but under longitudinal tension T. Steady, plane Poiseuille flow with flow rate q enters far upstream. The external pressure takes a constant value, p_e, referred to the pressure at the far end of the downstream rigid segment.

In all the following discussion, lengths are made dimensionless with respect to h_0, and the position of the membrane is given by

$$y = h(x,t), \quad 0 \le x \le L \tag{8}$$

where $h(0,t) = h(L,t) = 1$.

The first approach to this problem (Pedley, 1992) was based on lubrication theory, assuming negligible fluid inertia, steady flow and small wall slope: a one-dimensional model for low Reynolds number flow, but rationally derivable from the full equations of motion. The main innovation of that paper was its inclusion of the fact that the longitudinal tension in the membrane falls with downstream distance as a consequence of the viscous shear stress exerted by the fluid. However, the results were not qualitatively very different from the constant tension case, except when T fell close to zero. The main conclusion was that the steady problem has a solution, for all values of q and p_e, as long as T remains positive everywhere. For given positive values of longitudinal tension T_D and transmural pressure $p_e - p_D$ at the downstream end of the membrane (see figure 6), the membrane is collapsed everywhere ($h < 1$ for all $0 < x < L$) for sufficiently small flow rate q, but exhibits a bulge outwards at its upstream end when q exceeds a critical value q_b. In these respects, the conclusions are the same as from the high Reynolds number one-dimensional model discussed above.

Even for low Reynplds number flow, the lubrication theory analysis was not uniformly valid because the wall slope became large at the downstream end in cases for which T_D was small. The next stage was therefore a numerical solution of the Stokes equations, coupled to the membrane equations. This was performed iteratively by Lowe & Pedley (1995), who used the finite element method to solve for the flow with the membrane position assumed given, calculated the pressure and shear stress exerted on the membrane, and then updated the membrane position by requiring that the membrane equilibrium equations be satisfied, and so on. This procedure led to predictions of membrane shape, for given values of q, T_D and $p_e - p_D$, which agreed remarkably well with the lubrication theory results even when the wall slope was quite large, but failed to give a solution for sufficiently small (but positive) values of membrane tension. We attribute this failure at small T_D to a poor iteration scheme for very compliant boundaries.

We now formulate the general problem for unsteady flow, although the next computation to be described will be for steady flow at non-zero Reynolds number (Luo & Pedley, 1995). The full governing equations and boundary conditions for the unsteady problem, in dimensionless form, are as follows, where velocities are made non-dimensional with $u_0 = q/h_0$, time with h_0/U_0, stresses with ρU_0^2 (ρ is fluid density), and wall tension with $\rho U_0^2 h_0$; the Reynolds number is $Re = \rho U_0 h_0/\mu$ (μ is fluid viscosity) and the summation convention is used over suffixes $i, j = 1, 2$.

$$\text{Navier-Stokes} \quad u_{i,t} + u_j u_{i,j} = -p_i + Re^{-1} u_{i,jj} \tag{9a}$$

$$\text{Conservation of mass} \quad u_{i,i} = 0 \tag{9b}$$

Boundary conditions (refer to figure 6):
on $AB(x = -L_u)$

$$u_1 = 6y(1-y), \quad u_2 = 0 \tag{10a}$$

on $EF(x = L + L_d)$

$$-p + Re^{-1} u_{1,1} = 0, u_2 = 0 \tag{10b}$$

on $BC, DE, AF(y = 1$ for $x < 0$ or $x > L$; $y = 0$ for all $x)$

$$u_1 = u_2 = 0 \tag{10c}$$

on $CD(y = h(x,t), 0 \le x \le L)$

$$u_1 = u_2 = 0 \quad \text{(steady)} \tag{11a}$$

$$u_i = \text{velocity of membrane (unsteady)} \tag{11b}$$

$$p_e - \sigma_n = T h_{xx} (1 + h_x^2)^{-3/2} \tag{11c}$$

$$-\sigma_t = \partial T / \partial s. \tag{11d}$$

In the membrane equations (11c,d), σ_n and σ_t are the normal and tangential components of the stress exerted by the fluid on the membrane and s is the distance measured along the membrane. There should, in addition, be an equation relating the tension of each element of the membrane to its extension, but in this work we assumed that T is independent of time, t, which is equivalent to assuming that the tension is sufficiently large for length variations to cause negligible changes in T (but see section 3.2 below). That suggests that the tension is also sufficiently large for the longitudinal variation to be negligible, so from henceforth we ignore condition (11d) and take T in (11c) to be a constant. The computations have confirmed that the overall length changes are no more than $\pm 4\%$, even during the most vigorous oscillations found (Luo & Pedley, 1996).

Although the non-dimensionalisation described above is the most convenient for numerical solution, it is not convenient for the presentation of results because U_0 appears in the scalings for p_e and T. In presenting the results, therefore, we shall take

$$T = T_0 / \beta Re^2, \quad p_e = P_{e0} / \gamma Re^2, \tag{12}$$

where T_0 and p_{e0} are reference values, and increasing β or γ alone is equivalent to decreasing T or p_e at fixed Reynolds number Re.

Steady flow at finite Re was computed independently by Luo & Pedley (1995) and by Rast (1994), who both used the finite element method for the fluid flow, but used quite different techniques for coupling it to the membrane displacement. Luo & Pedley (1995) used the commercial flow solver FIDAP and iterated for the wall position in the manner described above in the context of Stokes flow. Rast (1994), on the other hand, used a finite element mesh which was coupled automatically to the membrane displacement by the method of spines (see Ruschak, 1980), and the membrane equation (11c) was discretised and solved simultaneously with the flow equations using Newton's method. The authors of both papers reported extensive accuracy tests, such as the effect of mesh refinement and adjustment of the location of the downstream boundary (i.e. the value of L_d), not only on membrane shape but also on the wall vorticity distribution, always one of the most sensitive tests of a CFD code. The best tests of all were agreement (a) between the results of the two computations and (b) with those of Lowe & Pedley (1994) at low Re.

Both approaches to the steady problem, like Lowe & Pedley (1995), failed to find a convergent solution for sufficiently small, but positive, values of T (or sufficiently large β: equation (12)). Luo & Pedley (1995) discussed whether the breakdown was associated with the corner singularity at the upstream end of the membrane (point C on figure 6) when the membrane began to bulge out there. (Note the appendix to Lowe & Pedley (1995), in which Moffatt's (1964) corner solution is extended to the case where one of the walls is a membrane under tension.) However, Rast (1994) and more recent computations of our own (Luo & Pedley, 1996) have found converged solutions with upstream bulging; breakdown occurs at a much lower tension (for given Re) than bulging. We have concluded that such problems are extremely ill-conditioned when the boundaries are highly compliant (cf. free-surface flow: Ruschak, 1980).

Steady flow results

Just the main features of the results will be presented here; more details can be found in the original papers. One general finding is that qualitatively similar behaviour is obtained when Re is increased at fixed tension (β) as when tension is decreased (β increased) at fixed Re. In what follows we fix Re at the value 300 and vary β. Other dimensionless parameters (chosen for comparison with previous papers) are taken to be: $L = 5$, $L_u = 5$, $L_d = 30$, $T_0 = 1.61 \times 10^7$, $p_{e0} = 9.3 \times 10^4$ and $\gamma = 1$.

The membrane displacement for various values of β is plotted in figure 7. At small β (large T) the membrane is stretched tight and is not deformed. As β is increased, the deformation increases, the minimum channel width h_{min} occurring close to the mid-point of the membrane. As the constriction becomes more severe, it tends to move downstream and a point of inflection appears in the upstream half. When β increases above about 30, two, possibly independent, phenomena are seen: the upstream part of the membrane begins to bulge out and the constriction, while continuing to move downstream, ceases to become more severe. In fact, h_{min} increases somewhat as β increases. The membrane slope becomes very large.

Both the above phenomena are also seen in the corresponding high-Reynolds-number one-dimensional model, which is exactly that of Jensen & Pedley (1989) described above (equations (5) and (6) plus $uA = q$) but with h for A and $\tilde{P}(A) \equiv 0$. Indeed, the shape of the graph of h_{min} against β predicted by that model is very similar to that given by the full computation, as shown in figure 8; the value of β at which bulging is first predicted is particularly close. The same is true at all Reynolds numbers from 50 to 500 (Luo & Pedley, 1995) though, as Re is decreased, h_{min} also falls, and occurs at larger β (smaller T). The one-dimensional model appears to be better than it deserves to be, at least in steady flow.

Unsteady results

Extension of the above studies to time-dependent flow and membrane displacement required extensive development of the computational scheme. The fully-coupled finite element method of Rast (1994) was extended to deal with time dependence. The mesh was taken to be time-dependent, but based on fixed spines; Newton's method was used to obtain convergence at each time step. Details are given in Luo & Pedley (1996). The main difficulty concerned the kinematic boundary condition (11b), because it is necessary to track boundary points as they move, and that is not possible in the absence of a description of membrane elasticity. The boundary condition was eventually based on the assumption that elements of the membrane always move in a normal direction; this is not strictly true, but is reasonable. To check the importance of this boundary condition, we compared the results with those obtained with the even simpler assumption that boundary points move only in the y-direction. This is clearly less satisfactory (e.g. near the downstream end of the membrane) but fortunately there was not much difference in the

results.

The unsteady code was used to investigate the stability of the steady solutions already computed (Luo & Pedley, 1996). The procedure was to start with a steady solution at a particular value of β, then increase the value of β a small amount and start the computation; the initial condition was therefore a small displacement from the steady solution at the new value of β. For values of β less than a critical value $\beta_c (\approx 27.5$ for $Re = 300)$ the perturbation dies away, revealing the steady solution to be stable. For $\beta > \beta_c$, the perturbation grew and finite-amplitude oscillations ensued, showing that there had been a Hopf bifurcation. Examples of the behaviour are given in figure 9, which shows the wall displacement h as a function of time at a fixed value of $x (x = 3.5$, close to the site of greatest constriction in the steady solution) and for three values of β. For $\beta = 30.0$, figure 9(a) shows an approximately sinusoidal oscillation, as is to be expected for a slightly supercritical value of β, with period 11.7 time units. However, for $\beta = 32.5$, figure 9(b) shows a few cycles of adjustment, followed by a (nearly) periodic oscillation, of period 21-25, in which large maxima and minima alternate with small ones. It seems clear that the system has gone through a period-doubling bifurcation. Finally, figure 9(c) shows the wall motion for $\beta = 35.0$; the wave-form is again more complex, indicating that at least one further bifurcation has occurred. We conclude that even this simple, two dimensional, constant-tension model is an interesting dynamical system which may well incorporate some of the complexities of real collapsible tube flow.

Effect of wall inertia

Real membranes have mass, so it is important to see whether wall inertia has a significant effect on the computed oscillations. Wall inertia can be included (approximately) by adding a term $-mh_{tt}$ to the right-hand side of equation (11c), where

$$m = \rho_w w / \rho h_0 \tag{13}$$

and ρ_w, w are the density and thickness of the membrane. Estimates for a thin rubber membrane suggest that $m = 0.01$ is a reasonable value when the flowing fluid is water and $m = 0.1$ or greater when it is air. The computations and results are described in detail by Luo and Pedley (1998). In brief, putting $m = 0.01$ makes essentially no difference to the results reported above, but $m = 0.1$ has a considerable effect. Examples are shown in figure 10. At $\beta = 30$ (figure 10a), the regular oscillations are set up as before, but are gradually swamped by a high-frequency flutter which eventually grows to such large amplitude that the code breaks down. Even at $\beta = 25$ (figure 10b), a previously stable state, high frequency flutter develops and grows large. These findings are consistent with those of experimentalists who have used air as well as water as the fluid flowing in a collapsible tube (e.g. Sakurai & Ohba (1986) compared with Ohba et al (1984)).

Streamlines and energy dissipation

We revert now to the case of no wall inertia, in an attempt to understand the mechanism of the instability and oscillations. In figure 11 we show the streamlines of the flow at various times during the oscillation cycle in just one case, that of $Re = 300$, $\beta = 32.5$ (figure 9b). The important point to note is that the flow separation downstream of the narrowest point does not occur always at or near that point, as it would if the flow were quasi-steady. Moreover, waves are seen to be generated and to propagate downstream in the rigid channel downstream of the oscillatory membrane. These are clearly the same as the vorticity waves observed and analysed by Pedley & Stephanoff (1985); not only do they look the same, but the wavelength $\lambda \approx 3.6$ of the nearly sinusoidal oscillations of period ≈ 11.5 at $\beta = 30$ is comparable in magnitude to those measured by Pedley & Stephanoff. Their run 5 with $Re = 487$ and the inverse of the dimensionless oscillation period, St, $= 0.77$ had wavelength ≈ 2.6; that was the shortest wavelength observed by those authors, corresponding to the highest value of St - theory suggests that $\lambda \propto St^{-1/3}$. [Note that what we call vorticity waves, because they are formed by the time-dependent, inviscid distortion of an oncoming flow with a non-zero vorticity gradient (cf. Rossby waves), are also an example of large-amplitude, inviscid Tollmien-Schlichting waves.] The streamline plots make it look as if the coupling between the vorticity waves and the flow separation process is somehow important for the latter, and hence for the separated flow energy loss that, according to the one-dimensional model, is a crucial feature in the system.

However, if we compute the rate of energy dissipation per unit volume, $\Phi = \mu u_{i,j}(u_{i,j} + u_{j,i})$, we are led in a different direction. Figure 12 shows contours of Φ for the same case and at the same times as the streamline patterns in figure 11. The remarkable feature is that, at almost all times, the highest rates of energy dissipation occur in viscous boundary layers, on the membrane and on the opposite wall *upstream* of the point of greatest constriction, not downstream as postulated by Cancelli & Pedley (1985) and used in the subsequent one-dimensional models. There are occasional pockets of high dissipation, at the edges of the primary separated eddy and associated with the vorticity waves, but most of the dissipation is upstream. The volume integral of Φ over four equal segments of tube $(0 < x < 4, 4 < x < 8, 8 < x < 12, 12 < x < 16)$ shows that the upstream segment contains the most dissipation all the time. The same is true for $\beta = 30$ (*a fortiori*), and for $\beta = 35$ except for a brief phase when the second segment, associated with the first separated eddy, has the most dissipation (see the corrigendum to Luo & Pedley (1996)).

A good physical explanation for the above findings still eludes us. Part of the difficulty is that the full time-dependent computations require very large computer resources, so we have not as yet examined parameter space in any detail.

3.2 The beam model

The membrane model described above contains a number of idealisations whose importance ought to be checked. In particular, it was assumed that the motion of a point on the membrane is always normal to the membrane, that the membrane has zero bending stiffness, and that the longitudinal tension in the membrane is constant. These assumptions have been relaxed in recent work by Cai & Luo (2003, 2005), whose computations have led to a surprising new result. These authors have replaced the constant-tension membrane equation (11c) by the Kirchhoff beam equations, whose dimensionless form is

$$\frac{m}{\lambda}\left(x_X x_{tt} + y_X y_{tt}\right) = c_\kappa \kappa \kappa_X + c_\lambda \lambda_X + \lambda \tau_n$$

$$\frac{m}{\lambda}\left(y_X x_{tt} - x_X y_{tt}\right) = c_\kappa \left(\frac{1}{\lambda}\kappa_X\right)_X - \lambda\kappa T - c_\lambda \lambda\kappa(\lambda - 1) - \lambda\left(\sigma_n - p_e\right)$$

where $x_X = \lambda\cos\theta$, $y_X = \lambda\sin\theta, \theta_X = \lambda\kappa$, θ being the angle made by the tangent to the beam with the x-axis; (x, y) is the current position of a point in the beam initially at $(X, 1)$; κ is the curvature: $\lambda = (x_X^2 + y_X^2)^{1/2}$ is the principal stretch ratio; and

$$\sigma_n = p - \frac{2}{Re}\frac{\partial u_n}{\partial n}, \quad \tau_n = -\frac{1}{Re}\left(\frac{\partial u_s}{\partial n} + \frac{\partial u_n}{\partial s}\right).$$

The quantity c_λ is proportional to the stretching stiffness (Young's modulus), while c_κ is proportional to the bending stiffness; m is the wall inertia parameter, and T is the initial tension when the beam is stretched but remains planar. Also the boundary conditions on the fluid velocity are now the correct no-slip and no-penetration conditions:

$$(u, v) = (x_t, y_t).$$

As in Luo's earlier work, the Navier-Stokes and beam equations are solved simultaneously, with inlet flow (Re) held fixed, on an adaptive mesh based on rotating spines.

Cai & Luo have investigated a number of parameter values; here we restrict ourselves to cases for which bending stiffness is expected to be negligible except in very small neighbourhoods of the beam ends, where the condition $\theta = 0$ is imposed, i.e. $c_\kappa \ll c_\lambda$. In fact, c_κ/c_λ is held fixed at the value 10^{-5}, and we also take $m = 0$, neglecting wall inertia. In the limit $c_\lambda \to 0$, this problem reduces to that of the constant-tension membrane, as presented above apart from using the correct boundary condition.

The results for steady flow are indistinguishable from those already presented, the membrane shape varying gradually as c_λ is increased (at fixed T). When $c_\lambda < 1$ the unsteady results are also indistinguishable. However, when c_λ is increased significantly above 1, and then T is decreased, from a high value at which the steady flow is stable, a new phenomenon appears, as shown in figure 13. There is a critical value of T below which oscillations set in and grow, but as T is further decreased the oscillations disappear and a zone of stability is found, before a new instability sets in. For yet lower values of T the progression through period doubling to probable chaos is the same as for the membrane model. This phenomenon is found for all c_λ up to about 932 for $Re = 300$ (the value for which figure 13 was plotted). An independently conducted linear stability analysis gives neutral curves that coincide with the stability boundaries according to the nonlinear computations, which tends to confirm the finding as a real physical phenomenon not a numerical artefact. However the authors and I have not yet succeeded in understanding the physical mechanism at work here, despite having followed the neutral curves over a range of Reynolds numbers, and despite having replotted them in various ways — see figure 14, in which the neutral curve is plotted in $T_f - Re$ space, where T_f is the final tension in the corresponding steady solution, at the downstream end of the beam:

$$T_f = T + c_\lambda[\lambda(X = 1) - 1] \tag{14}$$

3.3 High Reynolds number asymptotics

Another recent approach to understanding the two-dimensional membrane model of collapsible tube behaviour has been based on asymptotic analysis for high Reynolds numbers (Guneratne & Pedley, 2005). Here we follow the ground-breaking work of Smith (1976a,b), who analysed the perturbation to a steady Poiseuille flow in a channel encountering a slender, prescribed indentation in one or both walls (see also Pedley & Stephanoff (1985) for time-dependent indentations, and Pedley (2000) for a recent summary). The new feature here is the fact that the indentation shape is not prescribed in advance and has to be calculated as part of the solution.

At large Reynolds number (Re) the flow experiences a sideways displacement which is unaffected by viscosity except in boundary layers on the walls, of dimensionless thickness $\delta = O[(\lambda/Re)^{1/3}]$, where λ is the ratio of membrane length to channel width ($1 \ll Re^{1/7} \leq \lambda \ll Re$). The boundary layer equations are self-consistent if the membrane displacement $\epsilon = O(\delta)$, and their solution implies two relationships between the pressure gradient in the boundary layers, the core flow displacement A and the membrane displacement F. The membrane equation (11c) gives another relation from which, in principle, F can be calculated for any value of the membrane tension, T, and the transmural pressure $p - p_e$ (at the upstream end of the membrane, say), suitably non-dimensionalised. The most interesting feature of the steady-flow results is the fact that the solution to the problem is multiply non-unique, as shown in figure 15, if $|p - p_e|$ and T are sufficiently small. Many of these solutions will clearly be unstable, but their existence reinforces ones view of the collapsible tube or channel with flow through it as a complex and interesting dynamical system. Time-dependent solutions must be the subject of future work, as already begun in one region of parameter space by Jensen & Heil (2005).

Acknowledgements

Most of this review is taken from the paper by Pedley & Luo (1998). The author is extremely grateful to Dr Xiao-Yu Luo for her collaboration in the work described. He would also like to acknowledge the invaluable work of his other past and present collaborators in this area: Chris Bertram, Bindi Brook, Claudio Cancelli, Julie Guneratne, Matthias Heil, Tadashige Ikeda, Oliver Jensen, Roger Kamm, Tim Lowe, Mark Rast, Roger Seymour, Kyra Stephanoff, as well as many helpful conversations with Marc Bonis, Bill Conrad, Steve Cowley, Chris Davies, the late Sir James Lighthill, Yuji Matsuzaki, Kim Parker, the late Ascher Shapiro, and probably many others. The work described here has been supported by the UK Engineering and Physical Science Research Council and by the Universities of Leeds and Cambridge.

REFERENCES

Bertram, C.D. (1982) Two modes of instability in a thick-walled collapsible tube conveying a flow. *J. Biomech.* **15**, 223-224.

Bertram, C.D. (1986) Unstable equilibrium behaviour in collapsible tubes. *J. Biomech.* **19**, 61-69.

Bertram, C.D. & Pedley, T.J. (1982) A mathematical model of unsteady collapsible tube behaviour. *J. Biomech.* **15**, 39-50.

Bertram, C.D. & Pedley, T.J. (1983) Steady and un-

steady separation in an approximately two-dimensional indented channel. *J. Fluid Mech.* **130**: 315-345.

Bertram, C.D., Raymond, C.J. & Pedley, T.J. (1990) Mapping of instabilities during How through collapsed tubes of differing length. *J. Fluids & Structures* **4**, 125-154.

Bertram, C.D. Raymond, C.J. & Pedley T.J. (1991) Application of nonlinear dynamics concepts to the analysis of self-excited oscillations of a collapsible tube conveying a flow. *J. Fluids & Structures*, **5**, 391-426.

Bonis, M. & Ribreau, C. (1978) Etude de quelques propriétés de l'écoulement dans une conduite collabable. *La Houille Blanche* **3/4**, 165-173.

Brecher, G.A. (1952) Mechanism of venous flow under different degrees of aspiration. *Am. J. Physiol.* **169**, 423-433.

Brook, B.S., Falle, S.A.E.G. & Pedley, T.J. (1999) Numerical solutions for unsteady gravity-driven flows in collapsible tubes: evolution and roll-wave instability of a steady state. *J. Fluid Mech.* **396**, 223-256.

Brook, B.S. & Pedley, T.J. (2002) A model for time-dependent flow in (giraffe jugular) veins: uniform tube properties. *J. Biomech.* **35**, 95-107.

Brower, R.W. & Noordergraaf, A. (1973) Pressure flow characteristics of collapsible tubes: a reconciliation of seemingly contradictory results. *Ann. Biomed. Eng.*, **1** 333-335.

Brower, R.W. & Scholten, C. (1975) Experimental evidence on the mechanism for the instability of flow in collapsible vessels. *Med. Biol. Eng.*, **13**, 839-844.

Cai, Z.-X. & Luo, X.-Y. (2003) A fluid-beam model for flow in collapsible channels. *J. Fluids Struct.* **17**, 123-144.

Cai, Z.-X. & Luo, X.-Y. (2005) Stability of fluid-beam model for collapsible channel flow. (In preparation).

Cancelli, C. & Pedley, T.J. (1985) A separated flow model for collapsible tube oscillations. *J. Fluid Mech.* **151**: 375-404.

Conrad, W.A. (1969) Pressure-flow relationships in collapsible tubes. *IEEE Trans. BioMed. Eng.*, **BME-16**, 284-295.

Danaky, D.T. & Ronan,J.A. (1974) Cervical venous hums in patients on chronic hemodialysis. *New Engl. J. Med.*, **291**, 237-239.

Elad, D. & Kamm, RD. (1989) Parametric evaluation of forced expiration using a numerical model. *ASME J. Biomech. Eng.* **111**, 192-199.

Flaherty, J.K, Keller, J.B. & Rubinow, S.I. (1972) Post-buckling behaviour of elastic tubes and rings with opposite sides in contact. *SIAM J. Appl. Math.* **23**, 446-455.

Fry, D.L. (1958) Theoretical considerations of the bronchial pressure-flow-volume relationships with particular reference to the maximum expiratory flow volume curve. *Phys. Med. Biol.* **3**, 174-194.

Griffiths, D.J. (1971) Hydrodynamics of male micturition I. Theory of steady flow through elastic-walled tubes. *Med. Biol. Eng.* **9**, 581-588.

Guneratne, J.C. & Pedley, T.J. (2005) High-Reynolds-number steady flow in a collapsible channel. (Submitted).

Guyton, A.C. (1962) 'Venous Return': Handbook of Physiology, Section 2, Circulation, Vol. II ed. by W.F. Hamilton and P. Dow, American Physiological Society, Washington D.C.

Hazel, A.L. & Heil, M. (2003) Steady finite-Reynolds-number flows in three-dimensional collapsible tubes. *J. Fluid Mech.* **486**, 79-103.

Heil, M. (1997) Stokes flow in collapsible tubes: computation and experiment. *J. Fluid Mech.* **353**, 285-312.

Heil, M. & Pedley, T.J. (1996) Large post-buckling deformations of cylindrical shells conveying viscous flow. *J. Fluids & Structures* **10**, 565-599.

Jensen, O.E. (1990) Instabilities of flow in a collapsed tube. *J. Fluid Mech.* **220** 623-659.

Jensen, O.E. (1992) Chaotic oscillations in a simple collapsible-tube model. *ASME J. Biomech. Eng.*, **144**, 55-59.

Jensen, O.E. & Heil, M. (2003) High-freqneucy self-excited oscillations in a collapsible-channel flow. *J. Fluid Mech.* **481** 235-268.

Jensen, O.E. & Pedley, T.J. (1989) The existence of steady flow in a collapsed tube. *J. Fluid Mech.* **206**, 339-374.

Kamm, R.D. & Pedley, T.J. (1989) Flow in collapsible tubes: a brief review. *ASME J. Biomech Eng.* **111**, 177-179.

Katz, A.I., Chen, Y. & Moreno, A.H. (1969) Flow through a collapsible tube. *Biophys. J.* **9**, 1261-1279.

Lambert, R.K. (1989) A new computational model for expiratory flow from nonhomogeneous human lungs. *ASME J. Biomech. Eng.* **111**.

Lighthill, J. (1975) *Mathematical Biofluiddynamics*, SIAM.

Lowe, T.W. & Pedley, T.J. (1995) Computation of Stokes flow in a channel with a collapsible segment. *J. Fluids & Structures*, **9** 885-905.

Luo, X.Y. & Pedley, T.J. (1995) A numerical simulation of steady flow in a 2-D collapsible channel. *J. Fluids & Structures*, **9**, 149-174.

Luo, X.-Y. & Pedley, T.J. (1996) A numerical simulation of unsteady flow in a 2-D collapsible channel. *J. Fluid Mech.*, **314**, 191-225. (corrigendum **324**, 408-409).

Luo, X.-Y. & Pedley, T.J. (1998) The effects of wall inertia on flow in a 2-D collapsible channel. *J. Fluid Mech.*, **363**, 253-280.

Moffatt, H.K. (1964) Viscous and resistive eddies near a sharp corner. *J. Fluid Mech.* **18**, 1-18.

Ohba, K., Yoneyama, N., Shimanaka, Y. & Maeda, H. (1984) Self-excited oscillation of flow in collapsible tubes. *Tech. Rep. of Kansai Univ.* **25**, 1-13.

Pedley, T.J. (1980) *The fluid mechanics of large blood vessels*, Cambridge Univ. Press.

Pedley, T.J. (1992) Longitudinal tension variation in collapsible channels: a new mechanism for the breakdown of steady flow. *ASME J. Biomech. Eng.*, **114**, 60-67.

Pedley, T.J. (2000) Blood flow in arteries and veins. In: *Perspectives in fluid mechanics*, ed. by G.K. Batchelor, H.K. Moffatt and M.G. Worster. Cambridge University Press, pp.105-158.

Pedley, T.J., Brook, B.S. & Seymour, R.S. (1996) Blood pressure and flow rate in the giraffe jugular vein. *Phil. Trans. R. Soc. Lond. B.* **351,** 855-866.

Pedley, T.J. & Luo, X.-Y. (1998) Modelling flow and oscillations in collapsible tubes. *Theor. Comput. Fluid Dyn.*, **10**, 277-294.

Pedley, T.J. & Stephanoff, K.D. (1985) Flow along a channel with a time-dependent indentation in one wall: the generation of vorticity waves. *J. Fluid Mech.* **160**: 337-367.

Permutt, S., Bromberger-Barnea, B. & Bane, H.N. (1963) Hemodynamics of collapsible vessels with tone. The vascular waterfall. *J. Appl. Physiol.* **18**, 924-932.

Rast, M.P. (1994) Simultaneous solution of the Navier-Stokes and elastic membrane equations by a finite-element method. *Int. J. Num. Meth. Fluids*, **19**, 1115-1135.

Ruschak, K.J. (1980) A method for incorporating free boundaries with surface tension in finite element fluid-flow simulators. *Int. J. Num. Meth. Eng.*, **15**, 639-648.

Sakurai, A. & Ohba, K. (1986) Self-excited oscillation of flow in collapsible tube, III. *Tech Rep. Kansai Univ.* **28**, 41-48.

Schoendorfer, D.W. & Shapiro, A.H. (1977) The collapsible tube as a prosthetic vocal source. *Proc. San Diego Biomed. Symp.*, **16**, 349-356.

Shapiro, A.H. (1977a) Steady flow in collapsible tubes, *ASME J. Biomech. Eng.*, **99**, 126-147.

Shapiro, A.H. (1977b) Physiologic and medical aspects of flow in collapsible tubes. *Proc. 6th Can. Congr. Appl. Mech.*, 883-906.

Smith, F.T. (1976a,b) Flow through constricted or dilated pipes and channels, Parts I & II. *Quart. J. Mech. Appl. Math.* **29**, 343-364 and 365-376.

Ur, A. & Gordon, M. (1970) Origin of Korotkoff sounds. *Am. J. Physiol.*, **218**, 524-529.

FIGURE CAPTIONS

Figure 1. Sketch of the "tube law" for a collapsible tube, relating transmural pressure $\tilde{P}$ and cross-sectional area A. Sketches of the cross-sectional shape are given for three regions of the curve.

Figure 2. Sketch of the standard laboratory experiment. P_1, Q_1 are pressure and flow rate upstream of the collapsible segment; P_2, Q_2 are pressure and flow rate downstream; P_u is total pressure far upstream; P_e is pressure in the chamber surrounding the collapsible segment. R_1 and R_2 represent the rigid pipes up- and downstream, whose resistance can be prescribed.

Figure 3. Pressure drop $p_1 - p_2$ along the collapsible segment, plotted against flow-rate q for three different conditions: (a) $p_u - p_e$ held constant (from Brecher, 1952); (b) $p_e - p_2$ held constant (from Bertram, 1986); (c) $p_e - p_d$ held constant (from Conrad, 1969).

Figure 4. Pressure, p_2, at the downstream end of the collapsible segment, plotted against time t during self-excited oscillations for various values of the governing parameters (from Bertram, et al. (1991)).

Figure 5. Stability boundaries for the first two modes of instability, plotted on the dimensionless $P - Q$ plane ($P \propto p_e - p_2; Q \propto q$), as predicted by the one-dimensional model of Jensen (1990). The Hopf bifurcations are subcritical where the curves are dotted, supercritical elsewhere; (i) and (ii) are mode crossing points.

Figure 6. Sketch of the two-dimensional model problem.

Figure 7. Predictions of steady membrane shape at $Re = 300$ and various values of tension parameter $\beta(\propto 1/T)$, from Luo & Pedley (1996).

Figure 8. Predictions of minimum channel width during steady flow, plotted against β for fixed $Re(= 300)$. Bold solid and broken curves, from the two-dimensional computations; fine solid and broken curves, from the one-dimensional model. The broken curves represent steady states that are subsequently found to be unstable. Circles mark the value of β at which upstream bulging first appears.

Figure 9. Membrane displacement h at fixed $x = 3.5$ as a function of time during self excited oscillations. $Re = 300$; (a) $\beta = 30.0$, (b) $\beta = 32.5$, (c) $\beta = 35.0$.

Figure 10. Membrane displacement h at $x = 3.5$ as a function of time t in the presence of wall inertia. Solid curves, $m = 0.1$; dotted curves, $m = 0.Re = 300$; (a) $\beta = 30.0$, (b) $\beta = 25.0$.

Figure 11. Streamline plots at various times during self-excited oscillations for $Re = 300$, $\beta = 32.5$.

Figure 12. Contours of energy dissipation rate for the same parameters and times as the streamlines of figure 11.

Figure 13. Neutral stability curves in the $T - c_\lambda$ plane for $Re = 300$. Shaded zones are zones of instability according to linear theory. Points refer to the full computations (ignore the lettering). Note the zone of stability between the two unstable zones. The results from the previous membrane model are shown on the line $c_\lambda = 0$. (From Cai & Luo (2005)).

Figure 14. The neutral stability curve in the $T_f - Re$ plane for $c_\lambda = 600$; T_f is defined in equation (14). (From Cai & Luo (2005)).

Figure 15. Bifurcation diagrams in which the membrane slope at $x = 0$ is plotted against dimensionless tension T, for $P \propto p(x = 0) - p_e = 0$ and ± 0.1. Multiple non-uniqueness can be seen, especially as $T \to 0$. (Adapted from Guneratne & Pedley (2005)).

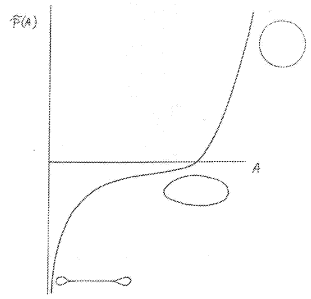

Fig 1

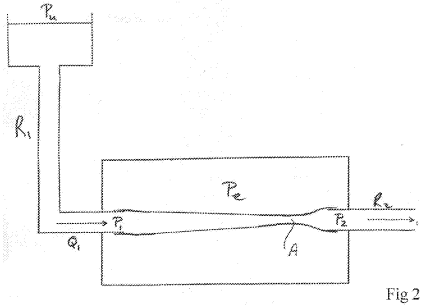

Fig 2

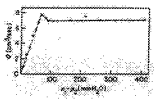

(a)

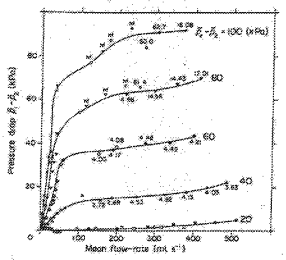

(b)

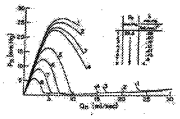

(c)

Fig 3

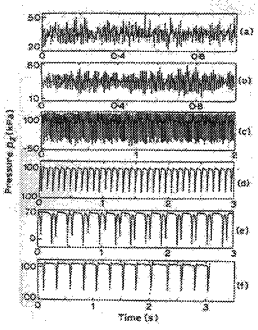

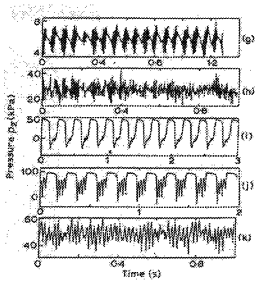

Fig 4

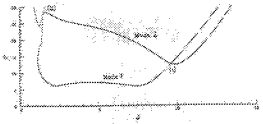

Fig 5

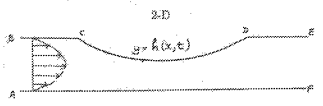

Fig 6

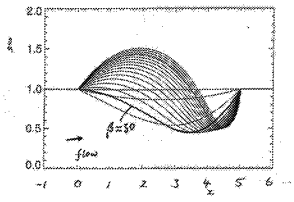

Fig 7

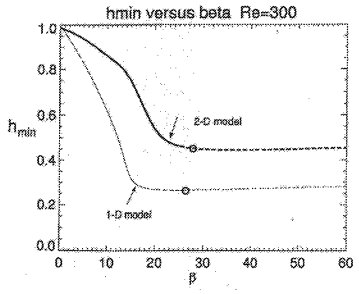

Fig 8

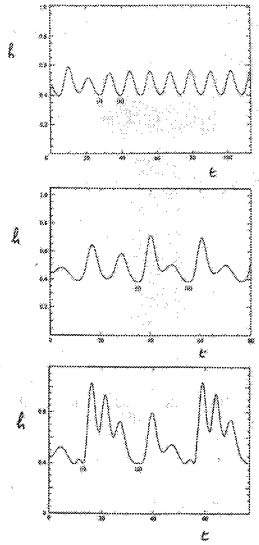

Fig 9

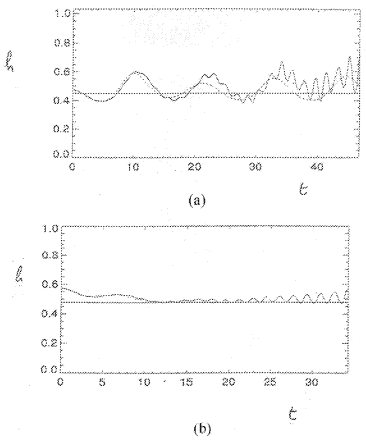

Fig 10

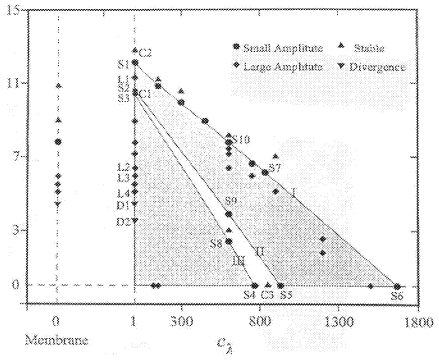

Fig 13

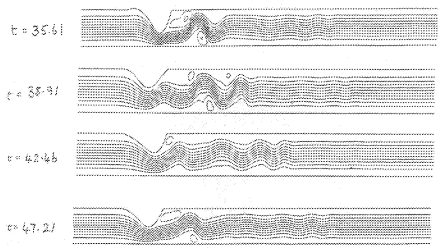

Fig 11

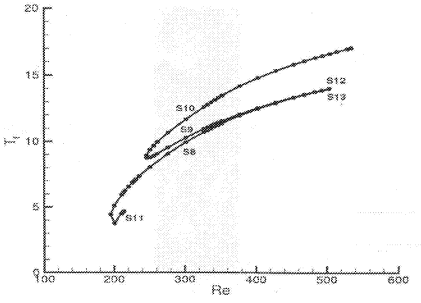

Fig 14

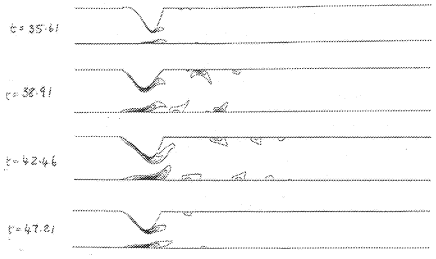

Fig 12

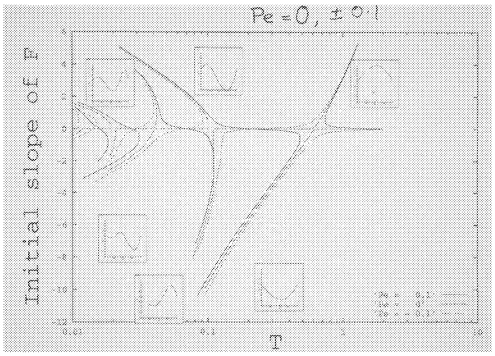

Fig 15